AAS 21-548

DEBRIS ATTITUDE EFFECTS ON ELECTROSTATIC TRACTOR RELATIVE MOTION CONTROL PERFORMANCE

Julian Hammerl* **and Hanspeter Schaub†**

The Electrostatic Tractor (ET) concept utilizes attractive Coulomb forces to relocate retired satellites from Geostationary Earth Orbit (GEO) to a graveyard orbit several hundred kilometers above GEO without any physical contact. Prior research investigated the charged relative motion control performance of the ET for two spherical spacecraft, and how electric potential uncertainty affects the control stability. This work utilizes the Multi-Sphere Method (MSM) to consider general three-dimensional spacecraft shapes, and investigates how the attitude of the debris and electric potential uncertainty affect the control effort and reorbit time. The results show that the reorbit time is minimized if protruding structures of the debris, such as solar panels, are directed toward the servicing satellite. The control effort, on the other hand, is only marginally affected by the debris attitude. Electrostatic torques generally cause the debris to tumble, and Monte Carlo simulations show that the rotation of the debris averages out the effects of debris attitude on control effort and reorbit time. However, the sensitivity of the controller to electric potential estimation errors is not entirely eliminated by a tumbling debris.

INTRODUCTION

An increasing number of satellites are located in Geostationary Earth Orbit (GEO). Despite international guidelines for space debris remediation,[1] many satellites reaching end-of-life are either reorbited to an insufficient distance away from GEO, or not reorbited at all.[2] This poses a risk to active satellites that take advantage of the unique assets of the geostationary belt. Several Active Debris Removal (ADR) methods have been investigated to either deorbit debris from Low Earth Orbit (LEO), or relocate objects from GEO to a graveyard orbit.[3,4] Most of these methods rely on physical contact, such as nets,[5] harpoons,[6] and robotic arms.[7] Nets and harpoons might create new fragments upon impact,[3] and the processes of docking or capture with robotic arms are made more complicated due to the high rotational rates of some large debris objects.[8,9]

The Electrostatic Tractor (ET) concept utilizes Coulomb forces to relocate geostationary debris to a graveyard orbit several hundred kilometers above GEO without any physical contact.[10] As illustrated in Fig. 1, a controlled servicing satellite emits an electron beam onto an uncooperative large debris object. Consequently, the servicer charges positively and the debris negatively. This results in an attractive electrostatic force between the two objects that acts like a virtual tethered connection. The servicing satellite is equipped with low-thrust inertial thrusters that are employed to raise the orbit altitude of the two-craft system. The risk of generating new debris fragments is

*Graduate Research Assistant, Ann and H.J. Smead Department of Aerospace Engineering Sciences, University of Colorado Boulder, Colorado Center for Astrodynamics Research, Boulder, CO, 80303 USA. julian.hammerl@colorado.edu

†Professor, Glenn L. Murphy Chair of Engineering, Ann and H.J. Smead Department of Aerospace Engineering Sciences, University of Colorado Boulder, Colorado Center for Astrodynamics Research, Boulder, CO, 80303 USA. AAS Fellow, AIAA Fellow

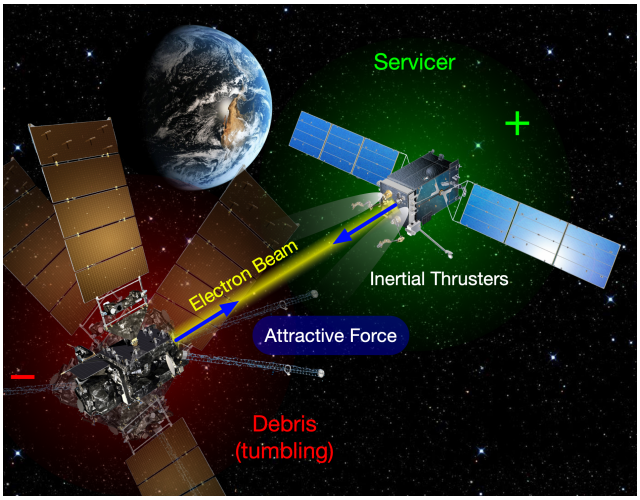

Figure 1: Electrostatic Tractor

smaller for the ET compared to other ADR concepts due to the contactless nature of the Electrostatic Tractor. A tumbling debris generally increases the fuel costs for docking, because the servicing satellite needs to match the relative rotation of the debris. Electrostatic forces, on the other hand, can be utilized to touchlessly detumble retired satellites.[11–13]

Prior research developed controllers for charged relative motion control of the ET for two spherical spacecraft and demonstrated that the orbit altitude can be increased by 300 km in two months.[14] The required control effort for the tugging process and the resulting reorbit time were computed, and the effects of charge uncertainty on the control stability were investigated. However, given the symmetric shape and charge distribution of a single sphere, attitude effects can not be considered if the single sphere is located at the center of mass of the corresponding object, and only translational effects were studied in Reference 14. The Multi Sphere Method (MSM) uses several spheres to represent complex shapes and approximates electrostatic forces between charged bodies with little computational effort.[15,16] This enables the consideration of complex spacecraft shapes and the resulting torques for research on charged astrodynamics.

More recent research examined the effects of electric potential uncertainty on the equilibria of the ET relative motion control for general three-dimensional spacecraft shapes using MSM.[17] If the electric potential uncertainty exceeds a critical value, the closed-loop relative motion control bifurcates and causes the two spacecraft to collide. Attitude state regions were identified where the relative motion is particularly sensitive to potential uncertainty. However, only the equilibria of the closed-loop response were investigated, without considering dynamical effects.

The focus of this work is to study the performance of the Electrostatic Tractor control for complex spacecraft models with general three-dimensional shapes. The effects of debris attitude on control effort and reorbit time are analyzed in two different ways. For the first type of analysis, different attitudes are prescribed to the debris and the reorbit process is simulated. This allows the identification of debris orientations that decrease or increase the control effort and reorbit time. The other type of analysis simulates the tugging process with a debris that is initially tumbling. Moreover, the effects of electric potential uncertainty on the dynamical performance of the ET relative motion control is investigated.

DYNAMICS MODEL

Relative Motion Dynamics

The relative motion dynamics are derived in Reference 14 in detail. The relative position of the debris with respect to the servicer is

$$\boldsymbol{\rho} = \boldsymbol{r}_D - \boldsymbol{r}_T \tag{1}$$

where $\boldsymbol{r}_D$ and $\boldsymbol{r}_T$ are the inertial position vectors of the debris and the servicer (tug T), respectively. Taking the inertial time derivative twice, using two-body gravitational acceleration for each satellite, and the total control acceleration $\boldsymbol{u}$ of the servicer, yields the relative equations of motion (EOM)

$$\ddot{\boldsymbol{\rho}} = -\frac{\mu}{r_D^3}\boldsymbol{r}_D + \frac{\mu}{r_T^3}\boldsymbol{r}_T + \boldsymbol{u} \tag{2}$$

with Earth's gravitational parameter $\mu = 3.986 \times 10^{14}$ m^3 s^{-2} and $r_D = |\boldsymbol{r}_D|$. The total control acceleration vector

$$\boldsymbol{u} = -\boldsymbol{F}_c\left(\frac{1}{m_T} + \frac{1}{m_D}\right) - \boldsymbol{u}_T \tag{3}$$

consists of the electrostatic force $\boldsymbol{F}_c$ between the servicer and the debris and the thruster control acceleration $\boldsymbol{u}_T$ due to the servicer's inertial thrusters. The mass of the debris and the tug are denoted by m_D and m_T, respectively. Using a Hill frame $\mathcal{H} : \{\hat{\boldsymbol{h}}_r, \hat{\boldsymbol{h}}_\theta, \hat{\boldsymbol{h}}_h\}$ with origin at the servicer's center of mass and

$$\hat{\boldsymbol{h}}_r = \frac{\boldsymbol{r}_T}{r_T}, \quad \hat{\boldsymbol{h}}_\theta = \hat{\boldsymbol{h}}_h \times \hat{\boldsymbol{h}}_r, \quad \hat{\boldsymbol{h}}_h = \frac{\boldsymbol{r}_T \times \dot{\boldsymbol{r}}_T}{|\boldsymbol{r}_T \times \dot{\boldsymbol{r}}_T|} \tag{4}$$

one expresses the relative position vector $\boldsymbol{\rho}$ in the Hill frame

$${}^{\mathcal{S}}\boldsymbol{\rho} = \begin{bmatrix} x \\ y \\ z \end{bmatrix} \tag{5}$$

and linearizes Eq. (2) to obtain:

$$\ddot{x} - 2n(t)\dot{y} - 3n^2(t)x = u_x \tag{6a}$$

$$\ddot{y} + 2n(t)\dot{x} = u_y \tag{6b}$$

$$\ddot{z} + n^2(t)z = u_z \tag{6c}$$

The Hill frame is inconvenient for control purposes since the equations are coupled in the x and y direction. Instead, a spherical frame $\mathcal{S} : \{\hat{\boldsymbol{s}}_L, \hat{\boldsymbol{s}}_\theta, \hat{\boldsymbol{s}}_\phi\}$ is implemented according to Fig. 2 with separation distance L between the tug and debris, in-plane rotation angle θ, and out-of-plane rotation angle ϕ.

Using the relations

$$L = \sqrt{x^2 + y^2 + z^2} \tag{7a}$$

$$\theta = \arctan\left(\frac{x}{-y}\right) \tag{7b}$$

$$\phi = \arcsin\left(\frac{-z}{L}\right) \tag{7c}$$

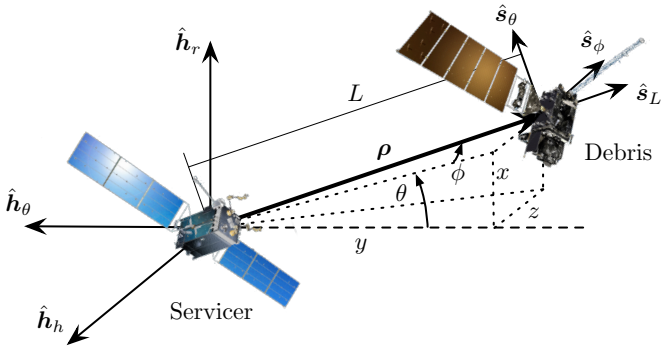

Figure 2: Hill frame $\mathcal{H}$ and Spherical frame $\mathcal{S}$

and

$$\begin{bmatrix} x \\ y \\ z \end{bmatrix} = \begin{bmatrix} L\sin\theta\cos\phi \\ -L\cos\theta\cos\phi \\ -L\sin\phi \end{bmatrix} \tag{8}$$

one obtains the spherical frame relative equations of motion:

$$\begin{bmatrix} \ddot{L} \\ \ddot{\theta} \\ \ddot{\phi} \end{bmatrix} = [\boldsymbol{F}(L,\theta,\phi,\dot{L},\dot{\theta},\dot{\phi})] + [G(L,\phi)]\,{}^{\mathcal{S}}\boldsymbol{u} \tag{9}$$

with

$${}^{\mathcal{S}}\boldsymbol{u} = \begin{bmatrix} u_L \\ u_\theta \\ u_\phi \end{bmatrix} \tag{10}$$

$$[\boldsymbol{F}] = \begin{bmatrix} \frac{1}{4}L\left(n^2\left(-6\cos(2\theta)\cos^2\phi + 5\cos(2\phi) + 1\right) + 4\dot{\theta}\cos^2\phi\left(2n+\dot{\theta}\right) + 4\dot{\phi}^2\right) \\ \left(3n^2\sin\theta\cos\theta + 2\dot{\phi}\tan\phi\left(n+\dot{\theta}\right)\right) - 2\frac{\dot{L}}{L}\left(n+\dot{\theta}\right) \\ \frac{1}{4}\sin(2\phi)\left(n^2\left(3\cos(2\theta)-5\right) - 2\dot{\theta}\left(2n+\dot{\theta}\right)\right) - 2\frac{\dot{L}}{L}\dot{\phi} \end{bmatrix} \tag{11}$$

and

$$[G] = \begin{bmatrix} 1 & 0 & 0 \\ 0 & \frac{1}{L\cos\phi} & 0 \\ 0 & 0 & -\frac{1}{L} \end{bmatrix} \tag{12}$$

Relative Motion Control

The feedback-control is developed in Reference 14

$${}^{\mathcal{S}}\boldsymbol{u} = [G(L,\phi)]^{-1}\Big(- [P]\dot{\boldsymbol{X}} - [K](\boldsymbol{X} - \boldsymbol{X}_r) - [\boldsymbol{F}(L,\theta,\phi,\dot{L},\dot{\theta},\dot{\phi})]\Big) \tag{13}$$

where it is shown that this control law is globally asymptotically stable. The desired steady-state values L_r, θ_r, ϕ_r are included in $\boldsymbol{X}_r$, $\boldsymbol{X} = [L,\theta,\phi]^T$, and $[K]$ and $[P]$ are positive definite gain

matrices. Solving Eq. (3) for the required thruster acceleration $\boldsymbol{u}_T$ and expressing all vectors in the spherical frame yields:

$$^{\mathcal{S}}\boldsymbol{u}_T = -^{\mathcal{S}}\boldsymbol{u} - {}^{\mathcal{S}}\boldsymbol{F}_{c,\text{est}} \left(\frac{1}{m_T} + \frac{1}{m_D} \right) \tag{14}$$

The thruster acceleration $\boldsymbol{u}_T$ is composed of a feedback term $\boldsymbol{u}$ and a feed-forward term of the estimated electrostatic force $\boldsymbol{F}_{c,\text{est}}$.

In this analysis, diagonal gain matrices $[K]$ and $[P]$ are chosen with the same feedback gain K_L for all states, such that $[K] = K_L[I]_{3\times3}$ with identity matrix $[I]_{3\times3}$. For a slightly underdamped response the diagonal elements P_i of $[P]$ are determined by $P_i = 1.85\sqrt{K_i}$.

Rotational Dynamics

The rotational dynamics of the debris are given by [18, Chapter 4]

$$[I]\dot{\boldsymbol{\omega}} = -[\tilde{\boldsymbol{\omega}}][I_D]\boldsymbol{\omega} + \boldsymbol{L}_c \tag{15}$$

where $\boldsymbol{\omega}$ is the angular velocity vector of the debris, $[\tilde{\boldsymbol{\omega}}]$ is the skew-symmetric matrix of $\boldsymbol{\omega}$ and is used as the cross-product equivalent matrix operator, $[I_D]$ is the inertia matrix of the debris, and $\boldsymbol{L}_c$ is the torque that acts on the debris due to the electrostatic forces. The debris satellite used in this analysis is based on a GOES-R satellite. Using publicly available information regarding the mass and size of this spacecraft, a CAD model is generated and the inertia matrix $[I_D]$ as well as the location of the center of mass are extracted.[19] The attitude of the servicing satellite is held constant at its nominal orientation during the simulation, so no rotational dynamics are required for the servicer.

Multi-Sphere Method

The Multi-Sphere Method (MSM) is implemented to approximate the charge distribution of objects with complex 3D shapes using a number of spheres.[15,16] For the Surface Multi-Sphere Method (SMSM), the spheres are distributed on the object's surface and the radii of the spheres are adjusted to match the self-capacitance of a higher-fidelity truth model that is obtained using the Method of Moments. The voltage to charge relationship for all spheres is given by

$$\begin{bmatrix} V_1 \\ V_2 \\ \vdots \\ V_n \end{bmatrix} = k_c \begin{bmatrix} 1/R_1 & 1/r_{1,2} & \cdots & 1/r_{1,n} \\ 1/r_{2,1} & 1/R_2 & \cdots & 1/r_{2,n} \\ \vdots & \vdots & \ddots & \vdots \\ 1/r_{n,1} & 1/r_{n,2} & \cdots & 1/R_n \end{bmatrix} \begin{bmatrix} Q_1 \\ Q_2 \\ \vdots \\ Q_n \end{bmatrix} \tag{16}$$

or

$$\boldsymbol{V} = [S]\boldsymbol{Q} \tag{17}$$

where V_i is the electric potential of the i-th sphere, R_i the radius, Q_i the electric charge, r_{ij} is the distance between the i-th and j-th sphere, and $k_c = 8.988 \times 10^9$ N m^2 / C^2 is the Coulomb constant. The matrix $[S]$ is called the elastance matrix. For two spacecraft, the voltage to charge relationship can also be expressed as

$$\begin{bmatrix} \boldsymbol{V}_1 \\ \boldsymbol{V}_2 \end{bmatrix} = \begin{bmatrix} S_1 & S_M \\ S_M^T & S_2 \end{bmatrix} \begin{bmatrix} \boldsymbol{Q}_1 \\ \boldsymbol{Q}_2 \end{bmatrix} \tag{18}$$

where S_M is the mutual capacitance block of the elastance matrix and S_1 and S_2 are the self-capacitance blocks of the spacecraft. Knowing the electric potential of each spacecraft (or sphere),

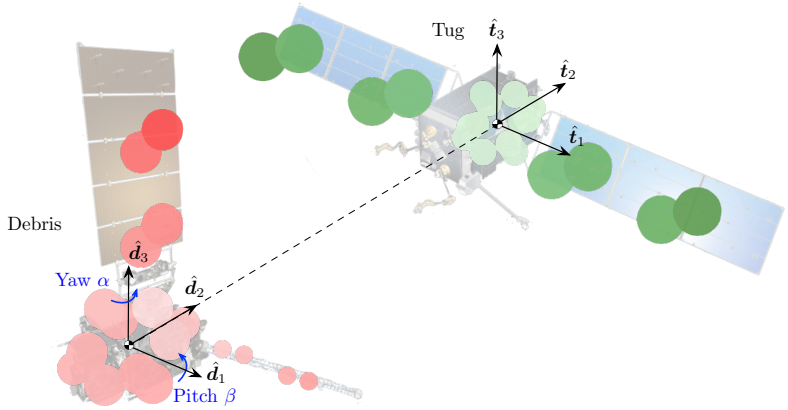

Figure 3: MSM Spacecraft models and spacecraft reference frames. The color of the MSM spheres indicates the electric charge: green corresponds to positive charge and red corresponds to negative charge; the stronger the color, the higher the charge magnitude

one of these equations is inverted to obtain the charge on each sphere. Once each charge is known, the electrostatic force and torque about point 0 acting on spacecraft 1 are computed by

$$\boldsymbol{F}_1 = -k_c \sum_{j=1}^{n_1} \boldsymbol{Q}_{1_j} \left(\sum_{i=1}^{n_2} \frac{\boldsymbol{Q}_{2_i}}{r_{i,j}^3} \boldsymbol{r}_{i,j} \right) \tag{19}$$

and

$$\boldsymbol{L}_{1,0} = -k_c \sum_{j=1}^{n_1} \boldsymbol{r}_j \times \boldsymbol{Q}_{1_j} \left(\sum_{i=1}^{n_2} \frac{\boldsymbol{Q}_{2_i}}{r_{i,j}^3} \boldsymbol{r}_{i,j} \right) \tag{20}$$

where $\boldsymbol{r}_j$ is the vector from point 0 to the j-th sphere.

Spacecraft Models

The spacecraft models used in this work are shown in Fig. 3, including the MSM models and the reference frame of each spacecraft. The debris is based on a GOES-R satellite and is chosen for its asymmetric shape due to the single solar panel and the magnetometer. An SSL-1300 satellite bus is used for the servicer. The $\mathcal{T} : \{\hat{\boldsymbol{t}}_1, \hat{\boldsymbol{t}}_2, \hat{\boldsymbol{t}}_3\}$ and $\mathcal{D} : \{\hat{\boldsymbol{d}}_1, \hat{\boldsymbol{d}}_2, \hat{\boldsymbol{d}}_3\}$ frames define the reference frame of the servicer and debris, respectively, and the origin of each frame is located at the geometric center of the corresponding spacecraft bus. The nominal orientation of each spacecraft is shown in Fig. 3 and corresponds to the orientation where the direction cosine matrix (DCM) that maps from the Hill frame $\mathcal{H}$ to the servicer (or debris) reference frame $\mathcal{T}$ (or $\mathcal{D}$) is equal to the identity matrix. The orientation of the debris is described using a 3-1-2 (Yaw-Pitch-Roll) Euler Angle set. Only 20 spheres are used on each spacecraft, because this significantly reduces the computation time without a considerable loss of accuracy.[17]

Simulation Setup

The simulation is set up in the following way. The servicing spacecraft starts at the desired position $\boldsymbol{X} = \boldsymbol{X_r}$ with $\theta_r = 0$ and $\phi_r = 0$, and the attitude of the servicing is held constant at its

Table 1: Simulation Parameters

m_T	m_D	V_T	V_D	K_L	L_r	Δa
2000 kg	2857 kg	25 kV	-25 kV	1.356×10^{-7}	20 m	300 km

nominal orientation according to Fig. 3. The initial attitude of the debris varies from one analysis to the other, and the attitude is either prescribed (meaning that it is held at a constant orientation) or freely rotating according to the rotational dynamics given in Eq. (15). The debris is then reorbited to a graveyard orbit at an altitude of Δa above GEO, where the semimajor axis difference between the graveyard orbit and GEO is Δa. Table 1 shows the simulation parameters used in this analysis, where the feedback gain K_L is determined according to Reference 17 for a maximum expected electric potential estimation error of the debris of $\Delta\Phi_{\text{max}} = 10\ \%$. The electric potentials of the tug and the debris are denoted by V_T and V_D, respectively. Fully conducting spacecraft are assumed.

The *Basilisk* astrodynamics simulation framework is used for all simulations.[20] This open source software package uses a set of C/C++ modules, and the scripts are written in Python. The simulations are set up easily using the Python scripts, while the C/C++ based modules allow for fast computations. Basilisk is capable of computing the electrostatic forces between several spacecraft using the Multi-Sphere Method, which makes this software package especially appealing for work on charged astrodynamics.

DEBRIS ATTITUDE EFFECTS

Prescribed Attitude

To begin, the effects of the debris attitude on the performance of the Electrostatic Tractor are investigated for prescribed attitudes. The attitude of the debris is set using yaw α and pitch β according to Fig. 3, where $-180^\circ < \alpha < 180^\circ$ and $-90^\circ < \beta < 90^\circ$. This orientation of the debris is held constant throughout the entire simulation.

Figure 4 shows the time it takes to increase the semimajor axis of the debris orbit by 300 km, as a function of the yaw and pitch angle of the debris. For three orientations (dark blue regions) at $(\alpha = 0^\circ, \beta = -90^\circ)$ and $(\alpha = \pm 180^\circ, \beta = 90^\circ)$, the required reorbit time is significantly lower than for the other orientations. At these debris orientations, the solar panel of the debris is pointing toward the servicing satellite. Similarly, the reorbit time is generally lower at $\alpha = 90^\circ$, where the magnetometer is directed toward the servicer. Essentially, the center of charge of the debris is closer to the servicer for these orientations, which increases the electrostatic force between the two spacecraft. Due to the higher electrostatic force, the thurster acceleration in the opposite direction increases as well to prevent the servicer from coming closer to the debris (Eq. (14)). Thus, as a result of the higher inertial thrust, the two satellites reorbit faster.

The effect of the debris attitude on the required Delta-V of the servicer for the reorbit process is shown in Fig. 5, where the Delta-V is computed by

$$\Delta V = \int |\boldsymbol{u}_T| \, \mathrm{d}t \tag{21}$$

The required Delta-V is not affected as significantly by the debris orientation as the reorbit time, as the Delta-V varies by only about 1 m/s between the worst-case and best-case orientation and an

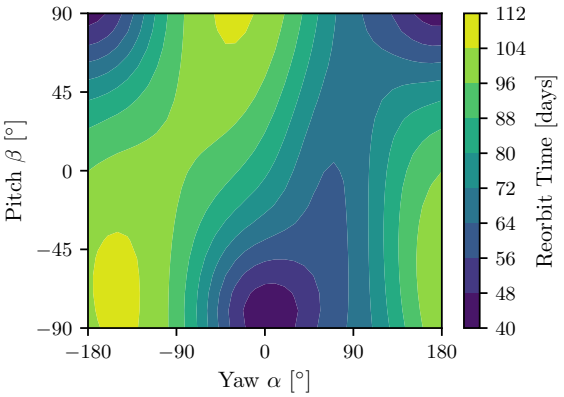

Figure 4: Reorbit Times for 300 km altitude raise with prescribed attitude

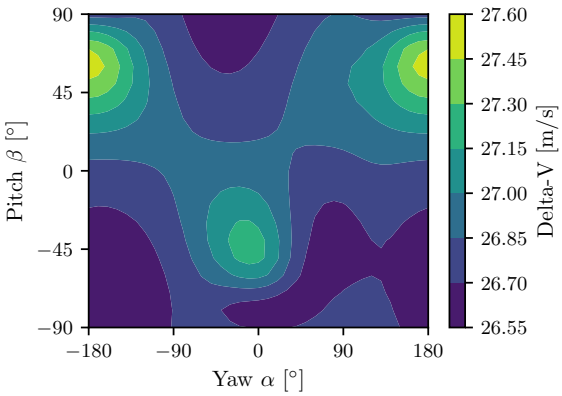

Figure 5: Delta-V for 300 km altitude raise with prescribed attitude

average of 26.84 m/s. Using the relation[10]

$$\frac{\mathrm{d}a}{\mathrm{d}t} = \frac{2a_\theta}{n} \tag{22}$$

with semi major axis a, along-track acceleration a_θ, and mean motion $n = \sqrt{\mu/a^3}$, the required Delta-V for an altitude raise of a single spacecraft is approximated by

$$\Delta V_{\text{single}} \approx \frac{1}{2}\sqrt{\frac{\mu}{a_0^3}}\Delta a \tag{23}$$

where it is assumed that $\Delta V_{\text{single}} = \int a_\theta \, \mathrm{d}t$. For an initial altitude of $a_0 = 42164$ km (GEO) and a semi-major axis increase of $\Delta a = 300$ km, this yields $\Delta V_{\text{single}} \approx 11$ m/s. The significantly higher ΔV of about 27 m/s for the ET is due to the fact that the servicing spacecraft is additionally pulling the debris, but the thrusters are only mounted to the servicer. In fact the required open-loop ΔV is about

$$\Delta V \approx \Delta V_{\text{single}} \frac{m_T + m_D}{m_T} = 26.71 \text{ m/s} \tag{24}$$

In a reorbiting scenario, one would like to minimize both the reorbit time and the required Delta-V. Figures 4 and 5 suggest that the ideal orientation for a GOES-R debris satellite is at $(\alpha = 0°, \beta = -90°)$, where the single solar panel of the GOES-R points toward the servicing satellite. Many retired satellites in GEO are tumbling,[9] so the debris must be detumbled and then held at the desired orientation. It has been proposed to touchlessly detumble objects in GEO using electrostatic forces.[11] The electrostatic detumble control has been investigated for target objects with cylindrical shapes[13,21] and satellite shapes including solar panels and magnetometers.[22] However, the main objective in these references is to reduce the angular velocity of the target object to a minimum such that docking becomes possible. That is, the object is detumbled without interest in the final attitude. Reference 23 demonstrates that it is possible to control the orientation (i.e. the final attitude after detumbling) of a cylindrical object using electrostatic forces, and the simulation results are validated experimentally. This provides a promising way of touchlessly holding the debris in a desired orientation to reduce both the required time and Delta-V budget while being reorbited with the Electrostatic Tractor.

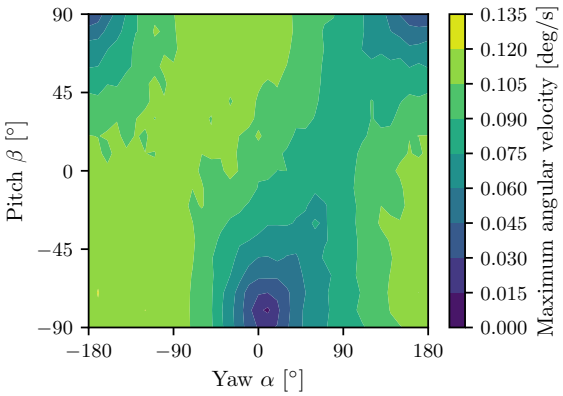

Figure 6: Maximum angular velocity during 300 km altitude raise

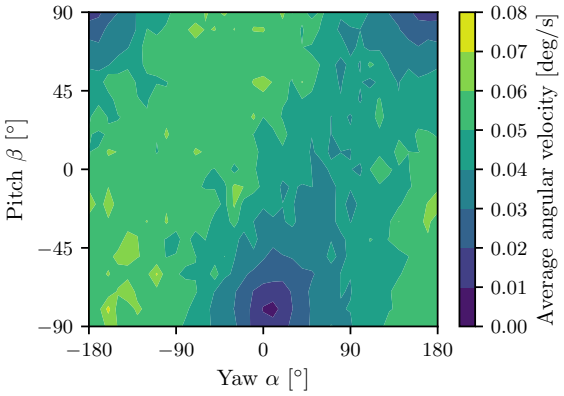

Figure 7: Average angular velocity during 300 km altitude raise

Freely Rotating Debris

Studying prescribed attitudes is valuable to identify optimal debris orientations for the Electrostatic Tractor concept. However, unless the attitude of the dysfunctional debris is externally controlled by the servicer using electrostatic forces and charge-control, the desired orientation of the debris can generally not be maintained. Moreover, one of the advantages of the ET compared to other ADR methods is that the debris does not need to be detumbled prior to reorbiting (some other ADR methods require low rotational rates of the debris to make capture with harpoons, nets or robotic arms possible). Thus, freely rotating debris are studied as well.

Similarly to the previous section, the initial orientation of the debris is set using yaw α and pitch β according to Fig. 3. However, the orientation of the debris is not held constant throughout the simulation as in the case for a prescribed attitude. Instead, the debris rotates freely according to the rotational dynamics given in Eq. (15).

For the first analysis, the simulation is started with no initial angular velocity of the debris. Figures 6 and 7 show the maximum and average angular velocity magnitude of the debris during reorbit. Overall, both figures look similar to Fig. 4: the maximum and average angular velocity magnitude is low for those initial orientations where protruding structures such as the solar panel or the magnetometer are directed toward the servicer, and high when these structures are initially pointing away from the servicer.

For conducting objects, electric charge generally accumulates at the corners and edges due to the repulsion of like charges within the object. Fully conducting spacecraft are assumed in this work, so electric charge gathers at the protruding solar panels of both spacecraft, as apparent in Fig. 3. Thus, for the GOES-R spacecraft model that is used as the debris here, the center of charge is shifted from the geometric center toward the solar panel. Note, however, that the charge distribution depends on the location and orientation of both satellites. The debris is subject to electrostatic torques if its center of charge does not align with its center of mass. The greater the distance from the center of charge of the debris perpendicular to the line that connects the center of mass of the debris with the center of charge of the servicer, the greater the torque. If, however, the center of charge of the debris lies on this line, no electrostatic torque is applied to the debris. This corresponds to the $\hat{\boldsymbol{s}}_L$ direction if the center of mass of each spacecraft aligns with the geometric center and the center of mass of the servicer coincides with its center of charge. This is visible in Figs. 6 and 7, as the maximum

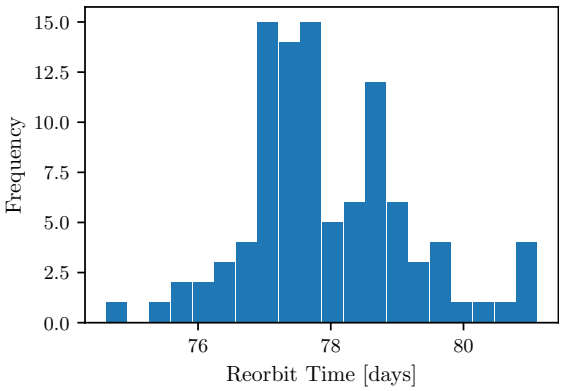

Figure 8: Histogram of Reorbit Times for 300 km altitude raise, 100 Monte Carlo runs. $\mu = 77.95$ days

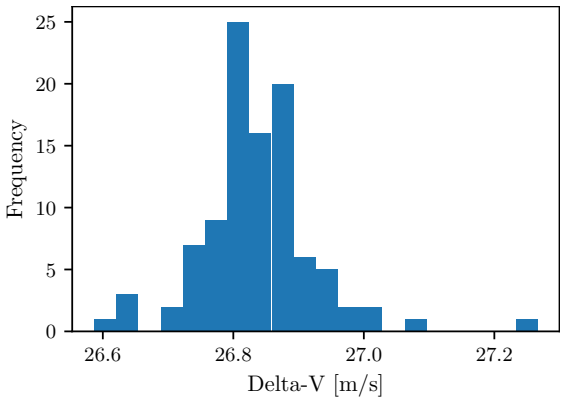

Figure 9: Histogram of Delta-V for 300 km altitude raise, 100 Monte Carlo runs. $\mu = 26.84$ m/s

and average angular velocity magnitude is low whenever the debris' initial orientation minimizes the perpendicular distance between the debris' center of charge and $\hat{\boldsymbol{s}}_L$ (e.g., when the solar panel points toward the servicer). A similar discussion on electrostatic torques is provided in Reference 24 for servicing and proximity operations.

This is advantageous for the case where one tries to hold the debris at a fixed attitude using charge-control of the servicer, because the orientation that is optimal for reorbit performance (solar panel pointing toward servicer) also results in a small electrostatic torque acting on the debris. While the specific favorable orientation strongly depends on the spacecraft shapes, this advantage is generally applicable. The reorbit time decreases with decreasing distance between the center of charge of each spacecraft due to the stronger electrostatic force. If the debris' center of charge lies on the line connecting each center of mass and on the side of the debris that is closer to the servicer, then both the reorbit time and the electrostatic torque are minimized.

For the second analysis, a Monte Carlo simulation with 100 runs is performed. Both the initial orientation and angular velocity are randomized (magnitude and direction) using uniform distributions. The initial angular velocity is bounded between 0 and 10 deg/s. Figures 8 and 9 show the histograms of the reorbit time and Delta-V. For the reorbit time, $\mu = 77.95$ days, which is slightly different than the average reorbit time in Fig. 4 of all prescribed attitudes $\mu = 81.45$ days. The mean of the Delta-V requirement is $\mu = 26.84$ m/s, and the average Delta-V of all prescribed attitudes in Fig. 5 is $\mu = 26.84$ m/s as well.

DEBRIS ATTITUDE EFFECTS INCLUDING ELECTRIC POTENTIAL ERROR

The control law in Eq. (14) includes a feed-forward term of the estimated electrostatic force. The electrostatic force depends on the electric potential of the debris, so an error in the estimated debris potential affects the control response.[14] The debris electric potential estimation error is defined as

$$\Delta\Phi = \frac{V_D - V_{D,\text{est}}}{V_D} \cdot 100 \tag{25}$$

where V_D is the electric potential of the debris and $V_{D,\text{est}}$ is the estimated potential. If the potential is under-estimated ($\Delta\Phi < 0$), the debris potential (which is already negative) becomes greater

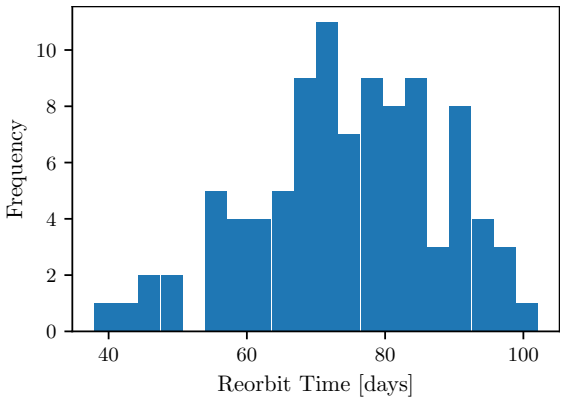

Figure 10: Histogram of Reorbit Times for 300 km altitude raise and randomized potential error, 100 Monte Carlo runs

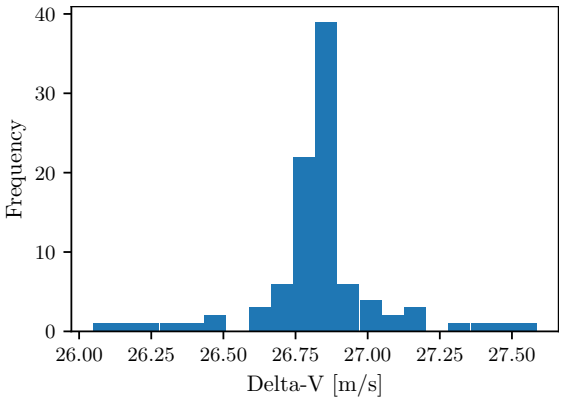

Figure 11: Histogram of Delta-V for 300 km altitude raise and randomized potential error, 100 Monte Carlo runs

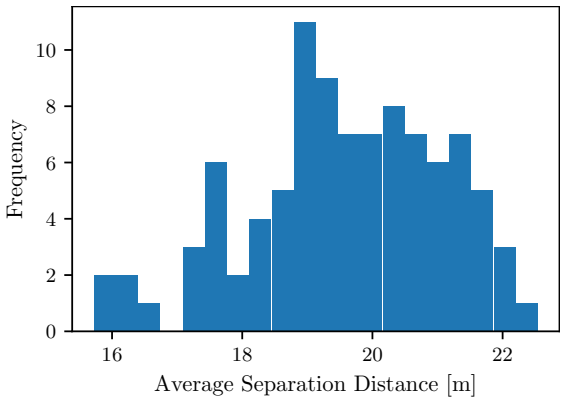

Figure 12: Histogram of Separation Distances for 300 km altitude raise and randomized potential error, 100 Monte Carlo runs

in magnitude and the electrostatic force is over-predicted. Consequently, the servicer settles at a distance that is greater than the desired separation distance. If the potential is over-estimated ($\Delta\Phi > 0$), on the other hand, the force is under-predicted and the servicer moves closer to the debris. An estimation error that exceeds a certain value causes the closed-loop response to bifurcate and the spacecraft collide. Reference 17 identifies debris orientations where the control response is especially sensitive to electric potential estimation errors. Even if the controller is set up to tolerate estimation errors up to 10 % (maximum expected estimation error), some debris orientations can cause the closed-loop response to bifurcate for estimation errors as low as 2 %. However, the authors focus on the equilibria of the relative motion control and not on the full dynamical response. Thus, the sensitivity of the control response to the identified orientations essentially corresponds to prescribed, fixed attitudes. As shown in the previous section, the debris generally starts to tumble due to the electrostatic torque if the center of charge is offset from the center of mass, so the sensitivity changes for a freely rotating debris.

To analyze the control sensitivity for a freely rotating debris, a Monte Carlo simulation with 100 runs similar to the simulation in the previous section is performed. Instead of assuming perfect

knowledge of the debris potential, a randomized estimation error is imposed that is sampled from a normal distribution with a mean μ of 0 and variance σ^2 of 25, that is $\Delta\Phi \sim \mathcal{N}(0, 25)$.

The histograms of the reorbit time, Delta-V requirement and average separation distance between the two spacecraft are shown in Figs. 10, 11 and 12. The separation distance deviates from the desired reference distance of 20 m due to the electric potential estimation error $\Delta\Phi$. Consequently, the reorbit time also varies to a greater extent than without any estimation error (see Fig. 8). The Delta-V requirement, however, remains more or less unaffected. Out of 100 simulation runs, the servicer collides with the debris in three cases due to an excessive estimation error (at $\Delta\Phi = 9.5\ \%, 9.6\ \%, 13.4\ \%$). The controller is set up to tolerate estimation errors of 10 % for the nominal spacecraft orientations (Fig. 3), but the critical estimation error at which the control response bifurcates is much lower for some orientations.[17] This suggests that the rotation of the debris reduces the sensitivity to estimation errors of the controller, because it is essentially averaged over several debris orientations. However, the issue of the bifurcation is not eliminated by the tumbling debris, as there are still cases where an estimation error of less than 10 % causes the spacecraft to collide. This issue can be solved by setting up the controller to tolerate an estimation error of 20 % at the nominal orientation, which is achieved by a higher feedback gain K_L.

CONCLUSIONS

This paper investigates the effects of the debris attitude on the reorbit time and Delta-V requirement of the Electrostatic Tractor (ET) active debris removal method. Complex spacecraft geometries including solar panels and spacecraft buses are implemented using the Multi-Sphere Method. The reorbit time is minimized if protruding structures of the debris (such as a solar panel) are pointing toward the servicing spacecraft, while the Delta-V requirement for the orbit altitude raise is marginally affected by the debris orientation. Thus, if one holds the debris at a desired attitude using remote electrostatic attitude control concepts, the reorbit time of the ET could be decreased. Further research is required to investigate how to hold an initially tumbling object with complex shapes at a desired orientation using electrostatic forces, as this has only been demonstrated for an axi-symmetric target object. If not controlled, the debris generally starts to tumble while being reorbited due to electrostatic torques. Monte Carlo simulations show that the rotation of the debris averages out the effects of debris attitude on control effort and reorbit time. The sensitivity of the relative motion control to estimation errors of the debris electric potential is decreased for a tumbling debris, but not eliminated. Thus, even for tumbling debris, higher feedback gains are recommended to reduce the sensitivity to electric potential estimation errors.

ACKNOWLEDGMENTS

This work was supported by U.S. Air Force Office of Scientific Research under grant FA9550-20-1-0025.

REFERENCES

[1] M. Yakovlev, "The "IADC Space Debris Mitigation Guidelines" and supporting documents," *4th European Conference on Space Debris*, Vol. 587, Darmstadt, Germany, 2005, pp. 591–597.

[2] S. Frey and S. Lemmens, "Status of the space environment: Current level of adherence to the space debris mitigation," *JBIS - Journal of the British Interplanetary Society*, Vol. 70, No. 2-4, 2017, pp. 118–124.

[3] M. Shan, J. Guo, and E. Gill, "Review and comparison of active space debris capturing and removal methods," *Progress in Aerospace Sciences*, Vol. 80, jan 2016, pp. 18–32, 10.1016/j.paerosci.2015.11.001.

[4] C. P. Mark and S. Kamath, "Review of Active Space Debris Removal Methods," *Space Policy*, Vol. 47, feb 2019, pp. 194–206, 10.1016/j.spacepol.2018.12.005.

[5] M. Shan, J. Guo, and E. Gill, "Deployment dynamics of tethered-net for space debris removal," *Acta Astronautica*, Vol. 132, mar 2017, pp. 293–302, 10.1016/j.actaastro.2017.01.001.

[6] R. Dudziak, S. Tuttle, and S. Barraclough, "Harpoon technology development for the active removal of space debris," *Advances in Space Research*, Vol. 56, aug 2015, pp. 509–527, 10.1016/j.asr.2015.04.012.

[7] S.-I. Nishida, S. Kawamoto, Y. Okawa, F. Terui, and S. Kitamura, "Space debris removal system using a small satellite," *Acta Astronautica*, Vol. 65, jul 2009, pp. 95–102, 10.1016/j.actaastro.2009.01.041.

[8] P. Papushev, Y. Karavaev, and M. Mishina, "Investigations of the evolution of optical characteristics and dynamics of proper rotation of uncontrolled geostationary artificial satellites," *Advances in Space Research*, Vol. 43, may 2009, pp. 1416–1422, 10.1016/j.asr.2009.02.007.

[9] J. Šilha, J.-N. Pittet, M. Hamara, and T. Schildknecht, "Apparent rotation properties of space debris extracted from photometric measurements," *Advances in Space Research*, Vol. 61, feb 2018, pp. 844–861, 10.1016/j.asr.2017.10.048.

[10] H. Schaub and D. F. Moorer, "Geosynchronous Large Debris Reorbiter: Challenges and Prospects," *The Journal of the Astronautical Sciences*, Vol. 59, jun 2012, pp. 161–176, 10.1007/s40295-013-0011-8.

[11] H. Schaub and D. Stevenson, "Prospects of Relative Attitude Control Using Coulomb Actuation," *The Journal of the Astronautical Sciences*, Vol. 60, dec 2013, pp. 258–277, 10.1007/s40295-015-0048-y.

[12] T. Bennett and H. Schaub, "Touchless Electrostatic Three-dimensional Detumbling of Large Axi-symmetric Debris," *The Journal of the Astronautical Sciences*, Vol. 62, sep 2015, pp. 233–253, 10.1007/s40295-015-0075-8.

[13] V. Aslanov and H. Schaub, "Detumbling Attitude Control Analysis Considering an Electrostatic Pusher Configuration," *Journal of Guidance, Control, and Dynamics*, Vol. 42, apr 2019, pp. 900–909, 10.2514/1.G003966.

[14] E. A. Hogan and H. Schaub, "Relative Motion Control For Two-Spacecraft Electrostatic Orbit Corrections," *Journal of Guidance, Control, and Dynamics*, Vol. 36, jan 2013, pp. 240–249, 10.2514/1.56118.

[15] D. Stevenson and H. Schaub, "Multi-Sphere Method for modeling spacecraft electrostatic forces and torques," *Advances in Space Research*, Vol. 51, jan 2013, pp. 10–20, 10.1016/j.asr.2012.08.014.

[16] J. A. Hughes and H. Schaub, "Heterogeneous Surface Multisphere Models Using Method of Moments Foundations," *Journal of Spacecraft and Rockets*, Vol. 56, jul 2019, pp. 1259–1266, 10.2514/1.A34434.

[17] J. Hammerl and H. Schaub, "Effects of Electric Potential Uncertainty on Electrostatic Tractor Relative Motion Control," *8th European Conference on Space Debris*, Darmstadt, Germany, apr 2021, pp. 1–13.

[18] H. Schaub and J. L. Junkins, *Analytical Mechanics of Space Systems*. Reston, VA: AIAA Education Series, 4th ed., 2018, 10.2514/4.105210.

[19] K. T. H. Wilson, *Remote Electrostatic Potential Determination for Spacecraft Relative Motion Control*. Doctoral thesis, University of Colorado Boulder, 2021.

[20] P. W. Kenneally, S. Piggott, and H. Schaub, "Basilisk: A flexible, scalable and modular astrodynamics simulation framework," *Journal of Aerospace Information Systems*, Vol. 17, No. 9, 2020, pp. 496–507, 10.2514/1.I010762.

[21] T. Bennett and H. Schaub, "Contactless electrostatic detumbling of axi-symmetric GEO objects with nominal pushing or pulling," *Advances in Space Research*, Vol. 62, dec 2018, pp. 2977–2987, 10.1016/j.asr.2018.07.021.

[22] F. Casale, H. Schaub, and J. Douglas Biggs, "Lyapunov Optimal Touchless Electrostatic Detumbling of Space Debris in GEO Using a Surface Multisphere Model," *Journal of Spacecraft and Rockets*, may 2021, pp. 1–15, 10.2514/1.A34787.

[23] D. Stevenson and H. Schaub, "Electrostatic spacecraft rate and attitude control—Experimental results and performance considerations," *Acta Astronautica*, Vol. 119, feb 2016, pp. 22–33, 10.1016/j.actaastro.2015.10.023.

[24] K. Wilson and H. Schaub, "Impact of Electrostatic Perturbations on Proximity Operations in High Earth Orbits," *Journal of Spacecraft and Rockets*, 2021, pp. 1–10, 10.2514/1.a35039.